EJSIT
European Journal of Science, Innovation and Technology
ISSN: 2786-4936
www.ejsit-journal.com
Volume 3 | Number 6 | 2023

Three-Dimensional Modeling of Pressure and Velocity Distribution in the Wide Edge Side Spillway Located in the Trapezoidal Channel

Zia Abidi
Civil Engineering, Froehling & Robertson, Maryland, USA

ABSTRACT

The flow in side spillways is turbulent, exhibiting a completely three-dimensional pattern. Due to the complexity of the flow and the effects caused by the scale, physical models alone are insufficient to provide an understanding of the physical requirements governing such overflows. It is necessary to numerically describe this phenomenon, and laboratory studies should be conducted in conjunction with the numerical investigation. In this research, the side spillway of the rectangular wide edge located in the trapezoidal earthen channel with a lateral slope of 1:2 has been simulated in three dimensions using the CFD method with Fluent Ansys. For modelling, the perturbation model (RNG) k-ε and the VOF numerical model have been employed. The values of pressure and velocity have been calculated at different points of the overflow. The results reveal alternating speed and pressure changes in the overflow, leading to the creation of two rotating currents emanating from the main channel into the side spillway. Additionally, subsequent to the side spillway, a subsidiary channel is formed.

Keywords: Wide edge side spillway, (RNG) k−ε, CFD, VOF model

INTRODUCTION

Spillways are among the oldest and simplest hydraulic structures, having been utilized for centuries by hydraulic engineers for various purposes such as measuring flow, energy loss, flow diversion, water depth regulation, flood control, and more (Jin et al., 2005; Yang et al., 2010). Side spillways find applications in irrigation, land drainage, flood control, urban drainage, and other areas. A side spillway is a specific type of overflow and free passage structure positioned on the side wall of a channel. If the length of the overflow crown is perpendicular to the axis of the river, it does not contribute to flood transfer (Rai et al., 2017a). However, when the flow level rises above the overflow crown, the lateral overflow efficiently diverts excess flow through a sub-channel. The water flow, having passed through the control section, enters the discharge channel with a 90-degree turn (Aliparast, 2009; Jeon et al., 2009). Subsequently, it is guided through the corresponding downstream channel of the dam. The flow inside the discharge channel and around the control section exhibits spatial variability, characterized by decreasing flow. Particularly, at the end of the control section, a critical state is observed within the discharge channel (Kazemzadeh-Parsi, 2014; Rai et al., 2017b). Since the beginning of the last century, the behavior of flow in side spillways has garnered significant attention, leading to numerous studies, primarily of an experimental nature.

Equations Governing the Flow

The water flow in side spillways represents a unique instance of spatially variable flow characterized by a decreasing discharge. The reduction in current within these overflows does not induce significant or specific changes, allowing the adjustment of the energy equation by setting the frictional drop to zero. The governing differential equations for this type of flow are as follows (Chanson, 2004):

$$\frac{dy}{dx} = \frac{S_o - S_o - \frac{\propto Q\,dQ}{gA^2\,dx}}{1 - \frac{\propto Q^2 T}{gA^3}} \quad (1)$$

In this relation, dy/dx represents the slope of the water level in relation to the bed. Here, y denotes the depth of the flow at each point, x indicates the distance in the direction of the overflow from the upstream end, S0 is the slope of the channel bottom, Sf is the frictional slope, Q stands for the discharge of the main channel, g is the acceleration due to gravity, A is the level of flow interruption, T is the width of the water surface, dQ/dx signifies the changes in flow rate along the channel, and α is the kinetic energy correction factor. Assuming a prismatic channel and a unit energy correction coefficient, the equation simplifies as follows:

$$\frac{dy}{dx} = \frac{Qy(-\frac{dQ}{dx})}{gB^2y^3 - Q^2} \quad (2)$$

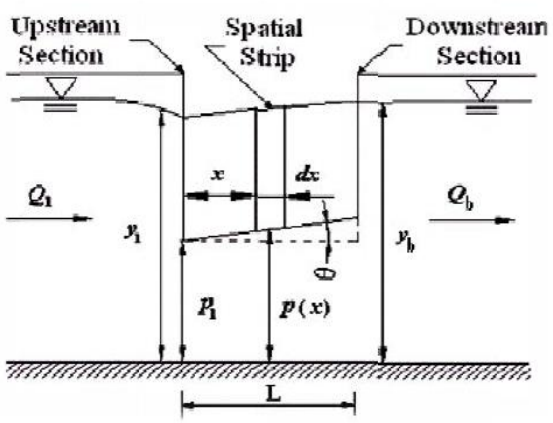

Figure 1. Cross-sectional view of the side spillway

B is the width of the main channel here.

Model k−ε (RNG)

In the RNG model, flow disturbance is determined through a precise statistical technique using mathematical relations. In this model, an additional term is incorporated into the ε equation, enhancing the accuracy of flow calculations. The governing equations in this model are as follows (Backhurst & Harker, 2001; Twort et al., 2000):

Equation k:

$$\rho \frac{dK}{dt} = \frac{\partial}{\partial x_i}\left[\left(\propto_k \mu_{eff}\right)\frac{\partial k}{\partial x_i}\right] + G_k - \rho\epsilon \quad (3)$$

Equation ϵ:

$$\rho \frac{D\epsilon}{Dt} = \frac{\partial}{\partial x_i}\left[\left(\propto_k \mu_{eff}\right)\frac{\partial k}{\partial x_i}\right] + C_{1\epsilon}\frac{\epsilon}{k}(G_k + G_{3\epsilon}) - C_{2\epsilon}\rho\frac{\epsilon}{k} - R \quad (4)$$

The R term, added to the ε equation in the RNG model compared to the standard state model, corrects this equation in areas with high strain rates. Leandro Spaulding presented the constants of the above equations based on the experimental data according to Table 1:

Table 1. Landrow Spalding's constant coefficients for K-ε equation (RNG)

C_μ	$C_{1\epsilon}$	$C_{2\epsilon}$		δ_ϵ
0.0845	1.42	1.68	1	1.30

Free Surface Model VOF

The free surface model was utilized by Nichol and Hirt in 1981. In determining the free surface, a variable called F is employed in addition to the fluid volume, as follows (Katopodes, 2019; Rubenstein et al., 2015):

$$\frac{\partial F}{\partial t} + \overline{U}\frac{\partial F}{\partial x} + \overline{V}\frac{\partial F}{\partial y} = 0 \quad (5)$$

In solving the equation in a fluid-filled with cells, the value of F is set to 1. In a cell devoid of fluid, this value is 0. For the cell specifying the free surface, this value falls between 0 and 1. In the present research, the value of F is considered as 0.75. While solving the governing equations to determine the fluid characteristics in half-filled cells, the obtained value of F in that cell is used to calculate and substitute the characteristics into the equations.

Numerical Solution of Equations

Ansys Workbench was employed for preparing the model's geometry and meshing. The model was built on a trapezoidal earthen channel, 30 meters long and 1 meter wide, with a side slope of 1:2. Additionally, a wide rectangular head, 4 meters long and 50 cm wide, was situated 13 meters from the channel's start. A set of experiments was undertaken by Kamyab Moghaddam and collaborators to assess static pressure in stepped chutes equipped with inclined and horizontal steps, and featuring end sills, under both nappe and skimming flow conditions. Their experimental setup utilized a model constructed from plexiglass, affixed to a steel frame, equipped with rows of piezometers to measure the pressure and obtained trustworthy results. In this study, we adopted a similar approach, employing the same roughness and material considerations for the numerical model. The obtained results were then compared to their findings, validating the accuracy of the model (Kamyab Moghaddam et al., 2023). The grid size was set at 0.1 m near the wall, on the crown, and in areas with changing flow regimes, while it was 0.15 m in other regions. It is crucial to note that the difference between the size of the largest and smallest cells in the network should not be significant for accurate and non-dispersive calculations. Figure 6 provides a snapshot of the meshing in the side spillway opening of the wide edge. Ansys Fluent flow analysis software was employed for solving the equations. Fluent treats the domain as separate control volumes, solving fluid flow equations for each. The two-phase system of water and air, along with the Volume of Fluid (VOF) method, is used to model the free surface (Khismatullin et al., 2006; Löhner et al., 2006). To discretize the pressure, the PRESTO scheme separates displacement terms using the Second Order Upwind scheme for momentum equations and the First Order Upwind scheme for turbulence equations. The SIMPLEC algorithm couples' pressure and velocity. The use of discount coefficients smaller than one for pressure, momentum, and Reynolds stresses prevents solution divergence. In this research, a permanent solution method and convergence criteria, with a relative error value of 0.0001 for each variable based on residual error, were chosen. Refer to Figure 2 for the model used in this research.

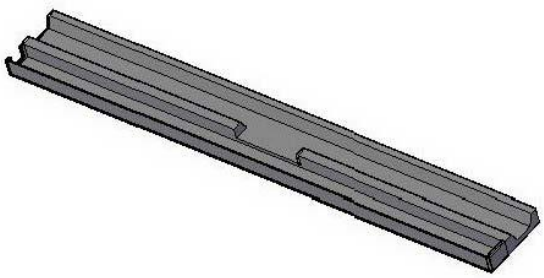

Figure 2. The view of the studied model includes the main channel, wide-edge side spillway, and sub-channel

Boundary Conditions

The outlet boundaries of the water channel were designated with the pressure-outlet boundary condition, and the velocity-inlet boundary condition was applied at the inlet. Walls were assigned the wall boundary condition. Additionally, the boundary between water and air was defined using the symmetry boundary condition.

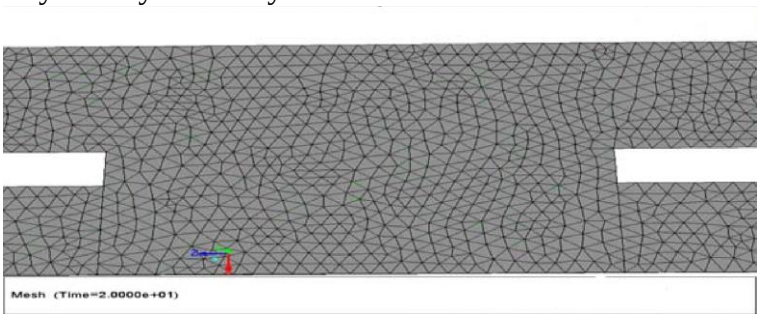

Figure 3. View of the grid of the solution field in the opening of the wide edge side spillway

RESULTS AND DISCUSSION

The three-dimensional pattern of the flow in the side spillway of the wide edge located in the trapezoidal channel was investigated using the (RNG)k-ε turbulence model and the VOF free surface model. Figures 4 and 5 depict pressure and velocity contours for the model. The flow entering the overflow possesses a strong momentum in the direction of the main channel, leading to the formation of a separation zone inside the overflow. Due to the presence of lateral pressure gradient and shear forces on the side of the center, the flow entering the side spillway becomes imbalanced, resulting in a clockwise rotating flow in the wide-edge side spillway. The same phenomenon occurs at the beginning of the flow entering the sub-channel. An examination of graphs depicting pressure changes and speed at different points of the overflow reveals that the flow has low speed at the beginning of entering the side spillway, with the speed increasing as it progresses along the route. Additionally, the pressure in the overflow decreases until the middle of the overflow and then increases, with the highest pressure occurring after the side spillway in the channel.

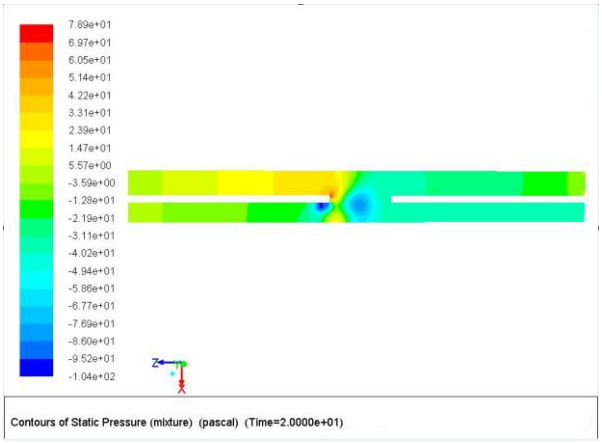

Figure 4. Pressure contours

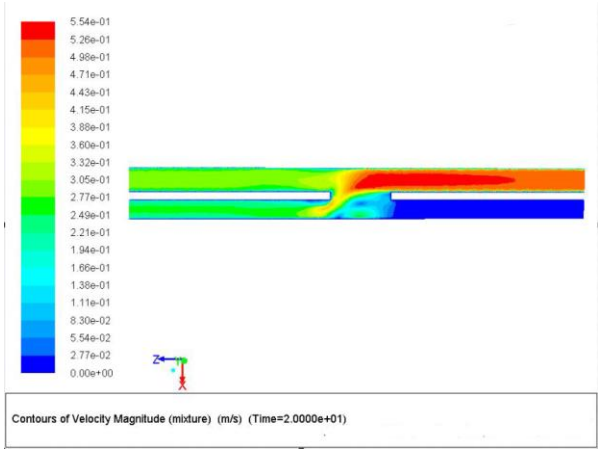

Figure 5. Speed contours

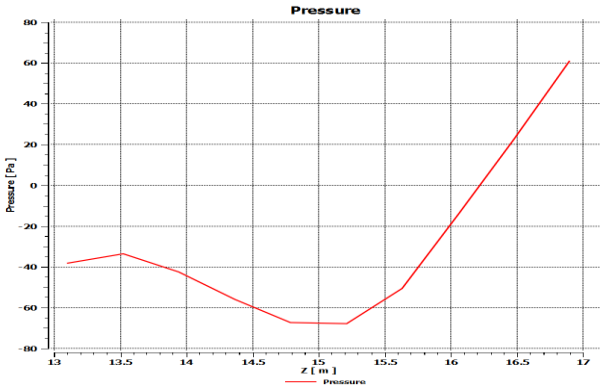

Figure 6. Pressure diagram at the side spillway inlet

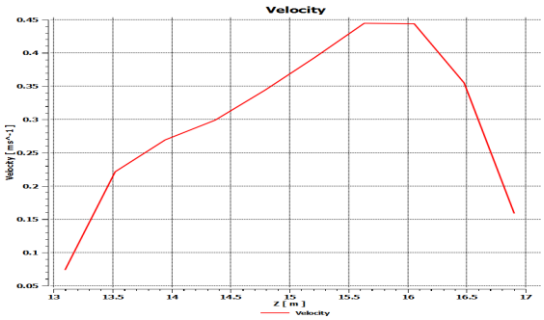

Figure 7. Velocity diagram at the entrance of the side spillway

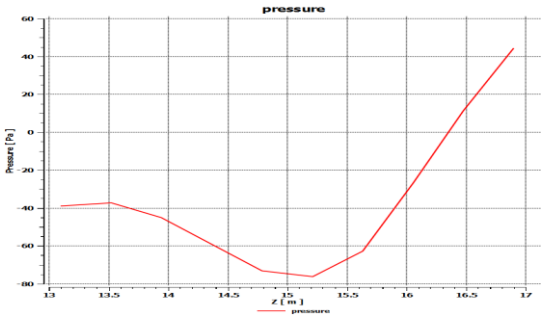

Figure 8. Pressure diagram in the middle of the side spillway

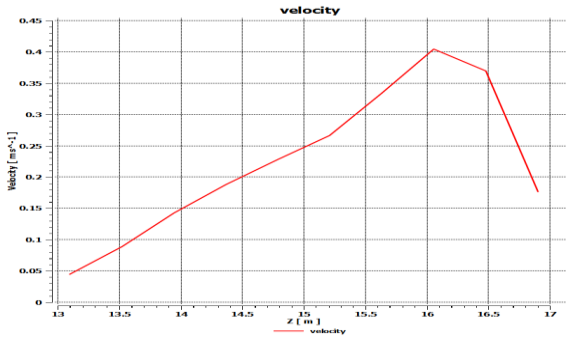

Figure 9. Velocity diagram in the middle of the side spillway

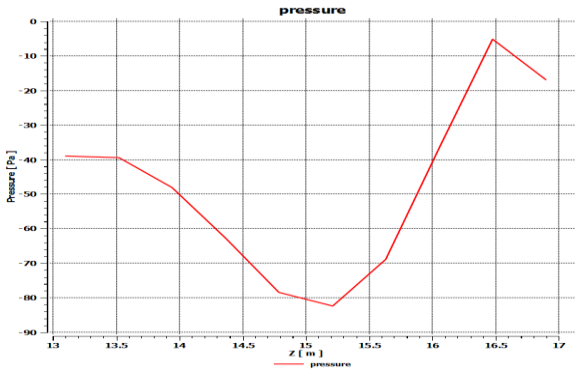

Figure 10. Pressure diagram at the end of the side spillway

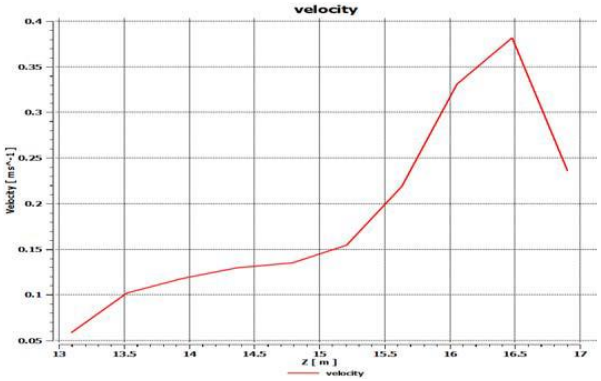

Figure 11. Velocity diagram at the end of the side spillway

REFERENCES

Aliparast, M. (2009). Two-dimensional finite volume method for dam-break flow simulation. *International Journal of Sediment Research*, *24*(1), 99–107. https://doi.org/10.1016/S1001-6279(09)60019-6

Backhurst, J. R., & Harker, J. H. (2001). SECTION 3—Flow in Pipes and Channels. In J. R. Backhurst & J. H. Harker (Eds.), *Chemical Engineering* (pp. 19–59). Butterworth-Heinemann. https://doi.org/10.1016/B978-0-08-049422-7.50007-9

Chanson, H. (2004). 2—Fundamentals of open channel flows. In H. Chanson (Ed.), *Environmental Hydraulics of Open Channel Flows* (pp. 11–34). Butterworth-Heinemann. https://doi.org/10.1016/B978-075066165-2.50034-5

Jeon, J., Lee, J., Shin, D., & Park, H. (2009). Development of dam safety management system. *Advances in Engineering Software*, *40*(8), 554–563. https://doi.org/10.1016/j.advengsoft.2008.10.009

Jin, C., Soltani, M., & An, X. (2005). Experimental and numerical study of cracking behavior of openings in concrete dams. *Computers & Structures*, *83*(8), 525–535. https://doi.org/10.1016/j.compstruc.2004.11.002

Kamyab Moghaddam, A., Hamedi, A., & Amirahmadian, S. (2023). Experimental survey of static pressure in stepped chutes with inclined and horizontal steps equipped with end sills in nappe and skimming flow regimes. *World Journal of Advanced Engineering Technology and Sciences*, *8*(2), 034–040. https://doi.org/10.30574/wjaets.2023.8.2.0069

Katopodes, N. D. (2019). Chapter 12—Volume of Fluid Method. In N. D. Katopodes (Ed.), *Free-Surface Flow* (pp. 766–802). Butterworth-Heinemann. https://doi.org/10.1016/B978-0-12-815485-4.00018-8

Kazemzadeh-Parsi, M. J. (2014). Numerical flow simulation in gated hydraulic structures using smoothed fixed grid finite element method. *Applied Mathematics and Computation*, *246*, 447–459. https://doi.org/10.1016/j.amc.2014.08.016

Khismatullin, D., Renardy, Y., & Renardy, M. (2006). Development and implementation of VOF-PROST for 3D viscoelastic liquid–liquid simulations. *Journal of Non-Newtonian Fluid Mechanics*, *140*(1), 120–131. https://doi.org/10.1016/j.jnnfm.2006.02.013

Löhner, R., Yang, C., & Oñate, E. (2006). On the simulation of flows with violent free surface motion. *Computer Methods in Applied Mechanics and Engineering*, *195*(41), 5597–5620. https://doi.org/10.1016/j.cma.2005.11.010

Rai, R. K., Singh, V. P., & Upadhyay, A. (2017a). Chapter 7—Design of Irrigation Canals. In R. K. Rai, V. P. Singh, & A. Upadhyay (Eds.), *Planning and Evaluation of Irrigation Projects* (pp. 283–318). Academic Press. https://doi.org/10.1016/B978-0-12-811748-4.00007-8

Rai, R. K., Singh, V. P., & Upadhyay, A. (2017b). Chapter 8—Design of Canal Outlets and Their Calibration. In R. K. Rai, V. P. Singh, & A. Upadhyay (Eds.), *Planning and Evaluation of Irrigation Projects* (pp. 319–339). Academic Press. https://doi.org/10.1016/B978-0-12-811748-4.00008-X

Rubenstein, D. A., Yin, W., & Frame, M. D. (2015). Chapter 2—Fundamentals of Fluid Mechanics. In D. A. Rubenstein, W. Yin, & M. D. Frame (Eds.), *Biofluid Mechanics (Second Edition)* (pp. 15–62). Academic Press. https://doi.org/10.1016/B978-0-12-800944-4.00002-0

Twort, A. C., Ratnayaka, D. D., & Brandt, M. J. (Eds.). (2000). 10—Hydraulics. In *Water Supply* (5th ed.) (pp. 463–498). Butterworth-Heinemann. https://doi.org/10.1016/B978-034072018-9/50012-6

Yang, M., Qian, X., Zhang, Y., Sheng, J., & Shen, D. (2010). Assessing Alternatives for Sustainable Management of A Flood Control Dam. *Procedia Environmental Sciences*, *2*, 98–110. https://doi.org/10.1016/j.proenv.2010.10.014